FEATURE ARTICLE

Relativity and Chemical Bonding

K. Balasubramanian[†]

Department of Chemistry, Arizona State University, Tempe, Arizona 85287-1604
(Received: January 13, 1989)

The importance of relativistic effects on chemical and spectroscopic properties of molecules containing very heavy atoms is considered. Recent developments that combine large scale ab initio multiconfiguration self-consistent field/configuration interaction (MCSCF/CI) methods with relativistic configuration interaction (RCI) methods including spin–orbit coupling effects are reviewed. The impact of relativistic effects on the electronic properties, geometries, dipole moments, and other properties of heavy-transition-metal clusters and their reactivities with H_2 are discussed. The periodic trends in properties and bonding within various groups are considered.

I. Introduction

Relativistic effects in chemical and spectroscopic properties arise from the difference in the true velocity of light as opposed to infinite velocity. In classical mechanics the velocity of light is assumed to be infinite and it is further assumed that light does not interact with the object of measurement. When the latter assumption is relaxed, nonrelativistic quantum mechanics is obtained through Heisenberg's uncertainty principle. The removal of both the assumptions leads to relativistic quantum mechanics. Relativistic corrections are then defined as the differences in the results obtained by using the true velocity of light as opposed to infinite velocity.

Nonrelativistic quantum mechanical methods based on ab initio techniques seem to be satisfactory for most of the molecules containing light atoms in the first two rows of the periodic table while these effects play a less important role for molecules containing third-row elements in comparison to the elements of other lower rows of the periodic table. The difference arises from the fact that the inner electrons of very heavy elements are subjected to such large nuclear charges that their speeds attain a considerable fraction of the speed of light. For example, the 1s electron of the gold atom attains 60% of the speed of light.

Relativistic effects become important for chemical properties when the inner electrons of the constituting atoms move with such high speeds as in the gold atom. Although the relativistic effects are substantially larger for the core electrons since these electrons are effectively subjected to larger nuclear charges, they manifest themselves in the valence space relevant to chemical bonding significantly to introduce substantial alterations in chemical bonding and valence spectroscopic properties of such molecules.

In recent years the impact of relativistic effects on chemical and spectroscopic properties has been the topic of discussions in a large number of investigations.[1-69] A striking impact of relativity is on the color of gold.[2] The outer 6s orbital of the gold atom contracts substantially due to a relativistic effect called the mass–velocity correction. The mass–velocity correction is essentially a relativistic correction in the kinetic energy arising from the variation of the mass of electron with speed as its speed approaches the speed of light. The very large relativistic corrections in the core manifest themselves in the valence space to a lesser extent, but substantially enough to alter the chemical and spectroscopic properties of gold-containing compounds. The contraction of the outer valence 6s orbital of the gold atom is large enough to induce enhanced stability and shorter bonds in gold clusters and compounds. The characteristic color of gold is attributed to an electronic transition from a nearly filled 5d band

[†] Camille and Henry Dreyfus Teacher–Scholar.

(1) Pitzer, K. S. *Acc. Chem. Res.* **1979**, *12*, 271.
(2) Pyykkö, P.; Desclaux, J. P. *Acc. Chem. Res.* **1979**, *12*, 276.
(3) Pyykkö, P. *Adv. Quantum Chem.* **1978**, *11*, 353.
(4) Desclaux, J. P. *At. Data Nucl. Data* **1973**, *12*, 311.
(5) Pyykkö, P., Ed. Proceedings of the Symposium on Relativistic Effects in Quantum Chemistry; *Int. J. Quantum Chem.* **1984**, *25*.
(6) Malli, G. L., Ed. *Relativistic Effects in Atoms, Molecules and Solids*; Plenum: New York, 1982.
(7) Krauss, M.; Stevens, W. J. *Annu. Rev. Phys. Chem.* **1984**, *35*, 357.
(8) Christiansen, P. A.; Ermler, W. C.; Pitzer, K. S. *Annu. Rev. Phys. Chem.* **1985**, *36*, 407.
(9) Balasubramanian, K.; Pitzer, K. S. *Adv. Chem. Phys.* **1987**, *67*, 287.
(10) Pyykkö, P. *Chem. Rev.* **1988**, *88*, 563.
(11) Schwarz, W. H. E. In *Theoretical Models of Chemical Bonding*; Maksič, Z., Ed., in press.
(12) Malli, G. *Stud. Phys. Theor. Chem.* **1982**, *21*, 199.
(13) McLean, A. D.; Lee, Y. S. *Stud. Phys. Theor. Chem.* **1982**, *21*, 219.
(14) Pitzer, K. S. *J. Chem. Soc., Chem. Commun.* **1975**, 760.
(15) Bagus, P. S.; Lee, Y. S.; Pitzer, K. S. *Chem. Phys. Lett.* **1975**, *35*, 408.
(16) Lee, Y. S.; Ermler, W. C.; Pitzer, K. S. *J. Chem. Phys.* **1977**, *15*, 5861.
(17) Lee, Y. S.; Ermler, W. C.; Pitzer, K. S. *J. Chem. Phys.* **1980**, *73*, 360.
(18) Christiansen, P. A.; Lee, Y. S.; Pitzer, K. S. *J. Chem. Phys.* **1979**, *71*, 4445.
(19) Lee, Y. S.; Ermler, W. C.; Pitzer, K. S.; McLean, A. D. *J. Chem. Phys.* **1979**, *70*, 288.
(20) Kahn, L.; Baybutt, P.; Truhlar, D. G. *J. Chem. Phys.* **1976**, *65*, 3826.
(21) Ermler, W. C.; Lee, Y. S.; Christiansen, P. A.; Pitzer, K. S. *Chem. Phys. Lett.* **1981**, *81*, 70.
(22) Pacios, L. F.; Christiansen, P. A. *J. Chem. Phys.* **1985**, *82*, 2664.
(23) Hurley, M. M.; Pacios, L. F.; Christiansen, P. A.; Ross, R. B.; Ermler, W. C. *J. Chem. Phys.* **1986**, *84*, 6840.
(24) LaJohn, L. A.; Christiansen, P. A.; Ross, R. B.; Atashroo, T.; Ermler, W. C. *J. Chem. Phys.* **1987**, *87*, 2812.
(25) Ermler, W. C.; Ross, R. B.; Christiansen, P. A. *Adv. Quantum Chem.* **1988**, *19*, 139.
(26) Pyykkö, P. *Relativistic Theory of Atoms and Molecules*; Springer-Verlag: Berlin and New York, 1986.
(27) Cohen, J. J.; Wadt, W. R.; Hay, P. J. *J. Chem. Phys.* **1979**, *71*, 2955.
(28) Hay, P. J.; Wadt, W. R. *J. Chem. Phys.* **1985**, *82*, 270.
(29) Wadt, W. R.; Hay, P. J. *J. Chem. Phys.* **1985**, *82*, 284.
(30) Hay, P. J.; Wadt, W. R. *J. Chem. Phys.* **1985**, *82*, 299.
(31) Christiansen, P. A.; Balasubramanian, K.; Pitzer, K. S. *J. Chem. Phys.* **1982**, *76*, 5087.

0022-3654/89/2093-6585$01.50/0

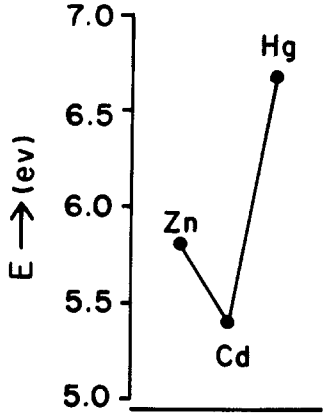

Figure 1. ^1S–^1P energy separations of Zn, Cd, and Hg.

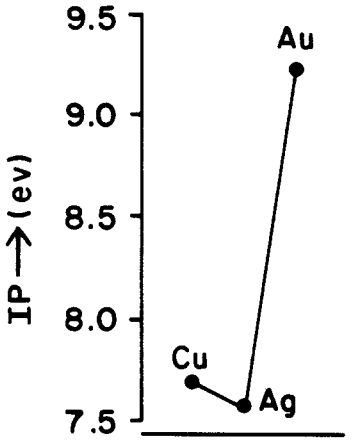

Figure 2. Ionization potentials of Cu, Ag, and Au.

to an essentially Fermi 6s band. Due to the stabilization of the 6s orbital, this band gap reduces to 2.4 eV in comparison to the corresponding gap in silver (3.5 eV).[2] Thus gold absorbs in the visible region, which leads to this characteristic color of gold.

The unusual stability of the mercurous ion, Hg_2^{2+}, is attributed to relativistic effects.[61] The mercurous ion (Hg_2^{2+}) is isoelectronic with Au_2 forming a $^1\Sigma_g^+$ (closed shell) ground state. The unusual stability of the 6s orbital due to the above-mentioned relativistic contractions leads to an "inert pair" effect, a phenomenon named

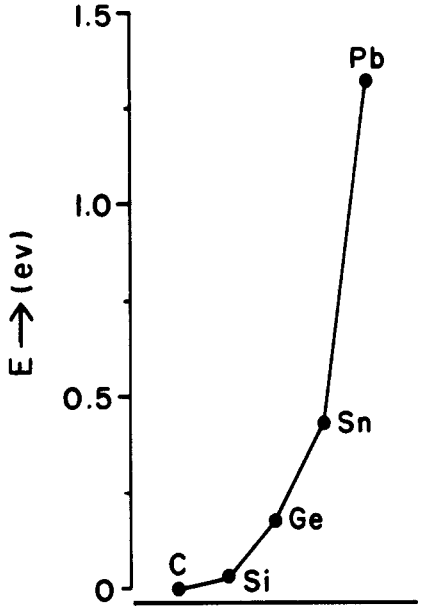

Figure 3. $^3P_0$–$^3P_2$ spin–orbit splittings for C–Pb.

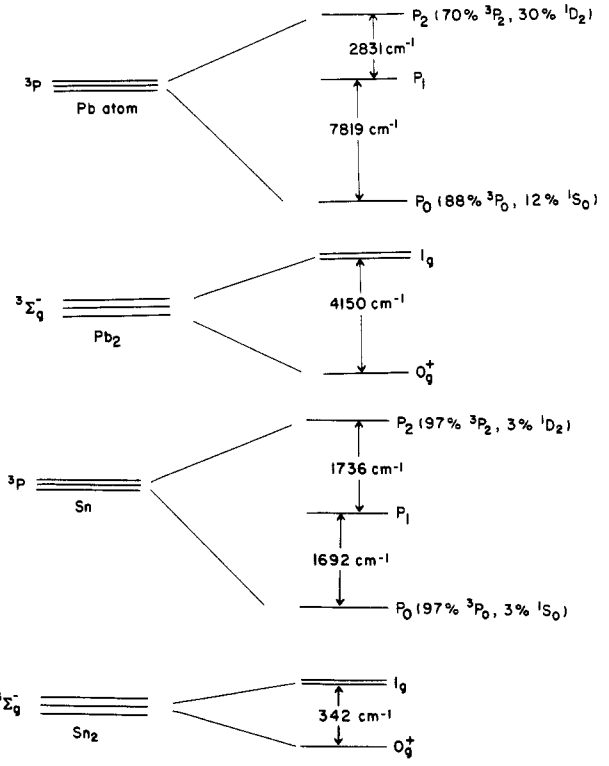

Figure 4. Spin–orbit splittings of the ^3P states of lead and tin atoms and $^3\Sigma_g^-$ states of Pb_2 and Sn_2. The atomic splittings are from ref 88 while the Pb_2 splitting is from ref 23.

(32) Balasubramanian, K.; Pitzer, K. S. *J. Chem. Phys.* **1983**, *78*, 321.
(33) Pitzer, K. S.; Balasubramanian, K. *J. Phys. Chem.* **1982**, *86*, 3068.
(34) Balasubramanian, K.; Pitzer, K. S. *J. Phys. Chem.* **1984**, *88*, 1146.
(35) Balasubramanian, K.; Pitzer, K. S. *J. Mol. Spectrosc.* **1984**, *103*, 105.
(36) Balasubramanian, K.; Pitzer, K. S. *J. Phys. Chem.* **1983**, *87*, 4857.
(37) Stevens, W. J.; Basch, H.; Krauss, M. *J. Chem. Phys.* **1984**, *81*, 6026.
(38) McLean, A. D. *J. Chem. Phys.* **1983**, *79*, 7.
(39) Lee, Y. S.; McLean, A. D. *J. Chem. Phys.* **1982**, *76*, 735.
(40) Ross, R. B.; Ermler, W. C. *J. Phys. Chem.* **1985**, *89*, 5202.
(41) Balasubramanian, K. *J. Phys. Chem.* **1984**, *88*, 5759.
(42) Balasubramanian, K. *J. Mol. Spectrosc.* **1986**, *115*, 258.
(43) Balasubramanian, K. *J. Chem. Phys.* **1985**, *82*, 3741.
(44) Balasubramanian, K. *Chem. Phys.* **1985**, *95*, 225.
(45) Chapman, D. A.; Balasubramanian, K.; Lin, S. H. *Chem. Phys. Lett.* **1985**, *118*, 192.
(46) Balasubramanian, K. *J. Chem. Phys.* **1985**, *83*, 2311.
(47) Balasubramanian, K. *Chem. Phys. Lett.* **1986**, *127*, 585.
(48) Balasubramanian, K. *Chem. Phys. Lett.* **1987**, *135*, 288.
(49) Balasubramanian, K.; Liao, M. Z. *J. Chem. Phys.* **1987**, *86*, 5587.
(50) Balasubramanian, K. *J. Chem. Phys.* **1987**, *87*, 2800.
(51) Balasubramanian, K.; Feng, P.; Liao, M. Z. *J. Chem. Phys.* **1987**, *87*, 3981.
(52) Chapman, D. A.; Balasubramanian, K.; Lin, S. H. *J. Chem. Phys.* **1987**, *87*, 5325.
(53) Balasubramanian, K.; Ravimohan, Ch. *J. Mol. Spectrosc.* **1987**, *126*, 220.
(54) Balasubramanian, K. *J. Chem. Phys.* **1987**, *87*, 6573.
(55) Balasubramanian, K.; Liao, D. W. *J. Chem. Phys.* **1988**, *89*, 317.
(56) Balasubramanian, K.; Liao, M. Z. *J. Phys. Chem.* **1988**, *92*, 361.
(57) Chapman, D. A.; Li, J. Q.; Balasubramanian, K.; Lin, S. H. *J. Chem. Phys.* **1988**, *88*, 3826.
(58) Balasubramanian, K.; Li, J. Q. *J. Mol. Spectrosc.* **1988**, *128*, 413.
(59) Balasubramanian, K.; Ravimohan, Ch. *Chem. Phys. Lett.* **1988**, *145*, 39.
(60) Balasubramanian, K.; Feng, P.; Liao, M. Z. *J. Chem. Phys.* **1988**, *88*, 6955.
(61) Niesler, R.; Pitzer, K. S. *J. Phys. Chem.* **1987**, *91*, 1084.
(62) Balasubramanian, K. *J. Chem. Phys.* **1988**, *89*, 5731.
(63) Balasubramanian, K.; Liao, D. W. *J. Phys. Chem.* **1988**, *92*, 6259.
(64) Balasubramanian, K. *J. Chem. Phys.* **1988**, *89*, 6310.
(65) Balasubramanian, K. *Int. J. Quantum Chem. Symp.* **1988**, *22*, 465.
(66) Balasubramanian, K.; Liao, M. Z. *Chem. Phys.* **1988**, *127*, 313.
(67) Balasubramanian, K.; Liao, M. Z. *J. Phys. Chem.* **1989**, *93*, 89.
(68) Balasubramanian, K. *J. Chem. Phys.* **1989**, *91*, 307.
(69) Wang, S. W.; Pitzer, K. S. *J. Chem. Phys.* **1983**, *79*, 3851.

for the inertness of the $6s^2$ and $6p^2$ shells in the bonding of the p-block elements of that row. Mercury is a liquid at room temperature while Cd and Zn are solids. This again is because of the fact that 6s–6p promotion energy is much larger for Hg in comparison to Cd and Zn. Figure 1 compares the periodic trend of the 6s–6p promotion energy by comparing the energy separations of the $(ns^2)^1S$–$(ns^1np^1)^1P$ states of these three atoms. All the atomic energy separations compared here are from atomic spectral information listed in Moore's books.[88] The comparison of ^1S–^1P separations of Zn, Cd, and Hg provides insight into the stabilization of the $6s^2$ shell. As seen from Figure 1, in going from Zn to Cd this separation decreases as expected since the energy splitting should decrease with increase in the principal quantum number. However, in comparing Cd with Hg we find a dramatic increase contrary to this expectation. This increase is, indeed, a consequence of relativistic stabilization of the $6s^2$ shell which leads to a larger ^1S–^1P separation for Hg in comparison to Cd. The $6s^2$ shell cannot thus form a very strong bond unless promotion into 6p is achieved. This is the reason for the fact that Hg_2 in its ground state forms only a van der Waals complex while in its excited state it is bound (excimer). Mercury is thus a liquid at room temperature.

Figure 2 compares the ionization potentials of Cu, Ag, and Au. Again, the expected trend is violated for the gold atom due to the enhanced stability of the gold 6s orbital in comparison to the 5s orbital of Ag.

The spin–orbit coupling term is another relativistic term that makes dramatic impact on energy separations and spectroscopic properties of molecules containing very heavy atoms. Figure 3 compares the $^3P_0$–$^3P_2$ spin–orbit splittings of atoms C through Pb in that group of the periodic table. As seen from this figure, there is a phenomenal increase in the spin–orbit splitting in comparing Sn (0.43 eV) to Pb (1.32 eV). It is thus very evident that relativistic effects increase substantially as one goes down the periodic table. The spin–orbit coupling term not only splits the electronic states of both atoms and molecules but also mixes electronic states of different symmetries that otherwise do not mix. Figure 4 compares the spin–orbit splittings of the ^3P ground states of the lead and tin atoms and the effects of spin–orbit coupling on the $^3\Sigma_g^-$ states of Pb_2 and Sn_2. Note that even the ground state of the lead atom is 88% $^3P_0$ and 12% $^1S_0$ in comparison to the tin atom, which is composed of 97% $^3P_0$ and 3% $^1S_0$.[32] Similarly, the $J = 2$ states of the two atoms are comprised by 70% $^3P_2$ and 30% $^1D_2$ for lead and 97% $^3P_2$ and 3% $^1D_2$ for tin. Consequently, it is clear that the coupling is intermediate for Pb. This large spin–orbit coupling in the very heavy atoms manifests itself in many ways

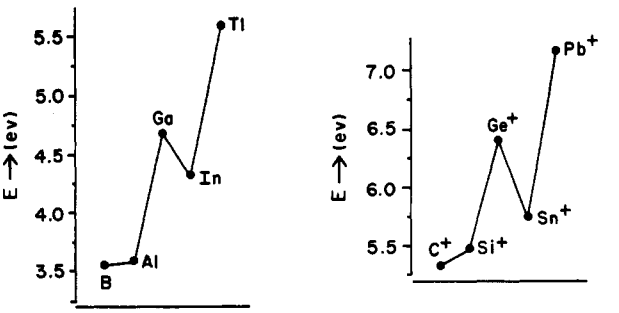

Figure 5. ^2P–^4P energy separations of B–Tl (left) and C^+–Pb^+ (right).

for molecules. For example, the dissociation energy, D_e, of Pb_2 is decreased to half of its value by the spin–orbit term.[32] The calculated D_es of Pb_2 and Sn_2 including the spin–orbit term are thus 0.88 and 1.86 eV, in excellent agreement with experimental values of 0.88 eV and 1.94 eV, respectively. Further, the 0_g^+ ground state of Pb_2 is a mixture of $^3\Sigma_g^-(0_g^+)(\sigma_g^2\pi_u^2)$, $^1\Sigma_g^+(0_g^+)(\pi_u^4)$, and $^1\Sigma_g^+(0_g^+)(\sigma_g^2\pi_u^2)$ whereas the ground state of Sn_2 is somewhat less contaminated by other states.

The spin–orbit contamination of different electronic states facilitates observation of electronic transitions that are normally forbidden. For example, the singlet–triplet electronic transition such as $^1\Sigma^+$–$^3\Pi$ is forbidden nonrelativistically. However, for molecules containing very heavy atoms, such transitions are very probable since transition moments are increased through spin–orbit contamination of different electronic states. For this reason the $B^3\Pi_u(0_u^+)$–$X^1\Sigma_g^+$ transition of I_2 becomes quite probable. The effect of spin–orbit coupling on dipole moments and transition moments will be one of the topics of this article.

Relativistic effects can both stabilize and destabilize chemical bonding. For example, the bonding in Au_2 is stabilized in comparison to Ag_2 by the relativistic mass–velocity contraction. On the contrary, as mentioned above, the bonding in Pb_2 is considerably weakened in comparison to Sn_2 due to the spin–orbit coupling. The unusual stability and ionic character of RnF (Rn^+F^-) is again due to the large spin–orbit interaction of Rn^+.[14]

The traditional explanation given for lanthanide contraction in inorganic chemistry textbooks is that it is due to incomplete screening of the 4f shells which leads to a gradual decrease of the atomic radii from La to Lu. However, the atomic Dirac–Fock calculations by Pitzer and co-workers[15] have demonstrated that about 30% of this contraction arises from relativistic effects.

A recent news article in *Chemical & Engineering News*[89] notes that relativity is used to plan chemical synthesis of gold-containing compounds. An unusually stable gold–carbon cation with octahedral structure, $[(C_6H_5)_3Au]_6C^{2+}$, was recently synthesized by Schmidbauer and co-workers[90] at Munich Technical University. The formation of six C–Au bonds is facilitated through relativistic contraction and stabilization of the 6s orbital of the gold atom.

The molecules Tl_2 and Pb_2 are weakly bound in comparison to their lighter analogs, viz., In_2 and Sn_2. To the contrary, PtH and Pt_2 are more stable in comparison to PdH and Pd_2. The weakening of bonds in the sixth-row p-block dimers is explained by the "inert pair effect" which is actually a consequence of relativistic effects. Figure 5 compares the $(ns^2np)^2P$–$(ns^1np^2)^4P$ energy separations of B–Tl and C^+–Pb^+. Note the dramatic increase in this separation for Tl and Pb^+. This, again, is a consequence of the relativistic mass–velocity stabilization of the $6s^2$ shell. The relativistic inert pair effect has a very interesting influence on the chemistry of the sixth-row p-block elements which will be discussed in this article.

The above survey clearly demonstrates the importance of relativity for molecules containing very heavy atoms. The objective of this article is to outline the recent advances in relativistic ab initio quantum mechanical calculations and their applications to very heavy transition-metal clusters, hydrides, and some main-

(70) Taylor, S.; Lemire, G. W.; Hamrick, Y.; Fu, Z.; Morse, M. D. *J. Chem. Phys.* **1988**, *89*, 4514.
(71) Ervin, K. M.; Ho, J.; Lineberger, W. C. *J. Chem. Phys.* **1988**, *89*, 4514.
(72) Walch, S. P.; Bauschlicher, C. W.; Langhoff, P. *J. Chem. Phys.* **1986**, *85*, 5900.
(73) Morse, M. D. *Chem. Rev.* **1986**, *86*, 1049.
(74) Smalley, R. E. In *Comparison of ab Initio Quantum Chemistry with Experiment*; Bartlett, R. J., Ed.; Reidel: Dordrecht, 1985.
(75) Weltner, W.; Van Zee, R. J. *Annu. Rev. Phys. Chem.* **1984**, *35*, 291.
(76) Geusic, M. F.; Morse, M. D.; O'Brien, S. C.; Smalley, R. E. *Rev. Sci. Instrum.* **1985**, *56*, 2123.
(77) Kappe, M. *Chem. Rev.* **1988**, *88*, 369.
(78) Cheschnovsky, O.; Pettiette, L. L.; Smalley, R. E. In *Ion Cluster Spectroscopy*; Maier, J. P., Ed.; Elsevier: Amsterdam, 1988.
(79) Brown, J. M.; Evenson, K. M.; Sears, T. J. *J. Chem. Phys.* **1985**, *83*, 3275.
(80) Petterson, L. G.; Langhoff, S. R. *Chem. Phys. Lett.* **1986**, *125*, 429.
(81) Werner, H. J.; Buckingham, A. D. *Chem. Phys. Lett.* **1986**, *125*, 433.
(82) Balasubramanian, K.; Li, J. Q. *J. Mol. Spectrosc.* **1988**, *128*, 413.
(83) Pitzer, R. M.; Winter, N. *J. Phys. Chem.* **1988**, *92*, 3061.
(84) The major authors of ALCHEMY II are B. Liu, B. Lengsfield, and M. Yoshimine.
(85) Brooks, B. R.; Schaefer, H. F. *J. Chem. Phys.* **1979**, *70*, 5092.
(86) Yoshimine, M.; Liu, B. *J. Chem. Phys.* **1988**, *74*, 612.
(87) Hafner, P.; Schwarz, W. H. E. *Chem. Phys. Lett.* **1979**, *65*, 537.
(88) Moore, C. E. *Tables of Atomic Energy Levels, Vol. I–III*; National Bureau of Standards, U.S. Government Printing Office: Washington, DC, 1971.
(89) Stinson, S. *Chem. Eng. News* **1988**, *66*, 6.
(90) Scherbaum, F.; Huber, B.; Kruger, C.; Schmidbaur, H. *Angew. Chem., Int. Ed. Engl.* **1988**, *27*, 1544; also see p 1542.

group compounds. Section II describes the various relativistic methods. The section on application is divided into several subsections dealing with a number of species. In this article I have endeavored to emphasize the impact of relativity on periodic trends. Thus, this article is not an overall review of the literature on these species.

II. Relativistic Methods

In earlier reviews[7-9] several relativistic methods have been outlined in considerable detail. In this article we outline in detail only the recent advances in this area after the appearance of these earlier reviews. However, the important earlier developments are described briefly to make this section understandable and self-explanatory.

Most of the modern relativistic quantum methods originate from the relativistic analogue of the Schrödinger equation called the Dirac equation. The main difference in the Dirac and Schrödinger equations is that the relativistic one-electron kinetic energy operator is quite different from the nonrelativistic operator due to the variation of the mass of the particle with its speed in the relativistic domain. The relativistic one-electron Dirac equation in a central Coulomb field is written as

$$\mathbf{H}_D\psi = \mathbf{E}\psi \tag{1}$$

where

$$\mathbf{H}_D = (\vec{\alpha}\cdot\vec{p} + C^2\beta - Z/r), \quad \alpha = \begin{pmatrix} 0 & \sigma_P \\ \sigma_P & 0 \end{pmatrix}, \quad \beta = \begin{pmatrix} \mathbf{I} & 0 \\ 0 & -\mathbf{I} \end{pmatrix} \tag{2}$$

where σ_Ps are the 2×2 Pauli matrices and $\mathbf{I}$ is the 2×2 identity matrix.

The Dirac Hamiltonian for a many-electron atom can be written as

$$\mathbf{H}_D = \sum_i h_D(i) + \sum_{i<j} \frac{1}{r_{ij}} \tag{3}$$

where $h_D(i)$ is the one-electron Dirac Hamiltonian

$$h_D(i) = \vec{\alpha}_i\cdot\vec{p}_i + \beta_i C^2 - Z/r_i \tag{4}$$

Since the above Hamiltonian consists of 4×4 matrices instead of simple scalar operators, the solution to the Dirac equation is a vector of four components known as a four-component spinor. It takes the form

$$\psi_{nkm} = \frac{1}{r}\begin{bmatrix} P_{nk}(r) & \chi_{km}(\theta,\phi) \\ iQ_{nk}(r) & \chi_{-km}(\theta,\phi) \end{bmatrix} \tag{5}$$

where

$$\chi_{km}(\theta,\phi) = \sum_{\sigma=\pm 1/2} C(l\,{}^1\!/_2\,j;m-\sigma,\sigma)\; Y_\lambda^{m-\sigma}(\theta,\phi)\phi_{1/2}^{\sigma} \tag{6}$$

$Y_\lambda^{m-\sigma}$ is a spherical harmonic,

$$\phi_{1/2}^{1/2} = \alpha = \binom{1}{0}; \quad \phi_{1/2}^{-1/2} = \beta = \binom{0}{1} \tag{7}$$

are the Pauli spinors, $C(l\,{}^1\!/_2\,j;m-\sigma,\sigma)$ are the Clebsch–Gordon coefficients, k is $(j + {}^1\!/_2)$ or $(-j - {}^1\!/_2)$, j is $l - {}^1\!/_2$ or $l + {}^1\!/_2$, and λ is k or $-(k + 1)$. In (5), the first two components P_{nk} are referred to as the large components while the second two components are called the small components. Although the small components make a significant contribution in the core region, the effect of these components in the valence region can be ignored. This was illustrated by a comparison of the relativistic and nonrelativistic radial solutions for the 6s orbital of Pb by Lee, Ermler and Pitzer.[16] Moreover, Schwarz[101] studied the effect of small components on the properties of molecules using the Foldy–Wouthuysen transformation and has shown that the contribution of the small components to chemical properties can be ignored.

The spinor nature of the wave function implies that, for example, in the $^2P_{1/2}$ state of the thallium atom, the p_z atomic orbital with an α-spin electron can mix with a p_x or p_y atomic orbital occupied by an electron with β spin. This leads to mixing of electronic states of different spatial symmetries and spin multiplicites. Similarly, the $J = 0$ ground state of the lead atom can be written in many ways, one of which is

$$({}^1\!/_2)^{1/2}\,({}^1\!/_2)^{-1/2} = \binom{p_0}{p_1}^{1/2}\binom{p_{-1}}{p_0}^{-1/2} = p_0\alpha p_{-1}\alpha + p_0{}^2 + p_1\beta p_{-1}\alpha + p_1\beta p_0\beta \tag{8}$$

The two-component approximation to the Dirac four-component spinor solution is also known as the Pauli approximation to the Dirac equation. As seen from (7) and (8), the first component of the two-component spinor represents the α spin while the second component describes the β spin. The two-component spinor approach can be envisaged as a way of introducing the spin–orbit coupling into electron structure calculations.

The idea of an atomic spinor approach can be extended to a molecular spinor approach by expressing molecular spinors as linear combinations of atomic spinors. An equivalent λ–s coupling picture can also be derived from the molecular spinors. For example, the $({}^1\!/_2)_g^{1/2}$ molecular spinor can be obtained by adding two $({}^1\!/_2)^{1/2}$p atomic spinors with same sign for a homonuclear diatomic. To illustrate

$$({}^1\!/_2)_1^{1/2} + ({}^1\!/_2)_2^{1/2} = ({}^1\!/_2)_g^{1/2} = \begin{pmatrix} \sigma_g \\ \pi_g^+ \end{pmatrix} = \sigma_g\alpha + \pi_g^+\beta \tag{9}$$

Note that the above expression implies mixing of a σ_g bonding orbital (spin α) with a π_g antibonding orbital (spin β). Similarly in the $({}^1\!/_2)_u^{1/2}$ spinor a σ_u antibonding orbital mixes with a π_u bonding orbital. This leads to destabilization of a bond that is primarily σ_g and stabilization of excited states in which, for example, there is considerable π_g antibonding, via mixing of σ_g bonding. This is the primary reason for spin–orbit destabilization of bonding in Pb_2 while it stabilizes the excited states.

Clusters and molecules made of very heavy atoms contain a large number of electrons, making all-electron calculations formidably difficult. In recent years, relativistic effective core potentials (RECP) methods have been developed.[7,16-24] The spirit of these methods is to replace the inner core electrons with relativistic effective core potentials (RECPs) and treat the valence electrons explicitly in these RECPs. The advantages of this method are elimination of core electrons, acceleration of convergence, facilitation of larger valence and Rydberg basis sets, and reduction of configurations in the CI.

The RECPs employed in conjunction with the multiconfiguration self-consistent field (MCSCF)/CI method have provided very good descriptions of the electronic and spectroscopic properties of molecules containing very heavy atoms. Pitzer and co-workers[16-24] have provided reliable RECPs derived from the relativistic Dirac–Fock calculations of very heavy atoms in these molecules. These potentials are derived from two-component spinors by ignoring the small components. The RECPs derived from the two-component spinors take the form

$$U^{REP} = U_{LJ} + \sum_{l=0}^{L-1}\sum_{j=|l-1/2|}^{l+1/2}\sum_{m=-j}^{j}[U_{lj}^{REP} - U_{LJ}^{REP}]|lmj\rangle\langle lmj| \tag{10}$$

(91) Balasubramanian, K.; Liao, D. W. *J. Phys. Chem.* **1989**, *93*, 3989.
(92) Cocke, D. L.; Gingerich, K. A. *J. Chem. Phys.* **1974**, *60*, 1958.
(93) Shim, I.; Gingerich, K. A. *J. Chem. Phys.* **1983**, *78*, 5693.
(94) Kant, A.; Strauss, B. *J. Chem. Phys.* **1964**, *41*, 3806.
(95) Hilpert, K.; Gingerich, K. A. *Ber. Bunsen-Ges Phys. Chem.* **1980**, *84*, 739.
(96) Balasubramanian, K.; Ravimohan, C. *J. Chem. Phys.* Submitted for publication.
(97) Scheiner, A. C.; Scuseria, G. E.; Rice, J. E.; Lee, T. J.; Schaefer, H. F. *J. Chem. Phys.* **1987**, *87*, 5361.
(98) Blomberg, M.; Brademark, V.; Petterson, L.; Siegbahn, P. *Int. J. Quantum Chem.* **1983**, *23*, 855.
(99) Low, J. J.; Goddard, W. A. *J. Am. Chem. Soc.* **1984**, *106*, 8321.
(100) Balasubramanian, K.; Ravimohan, C. *J. Phys. Chem.* **1989**, *93*, 4490.
(101) Schwarz, W. H. E. Private communication.

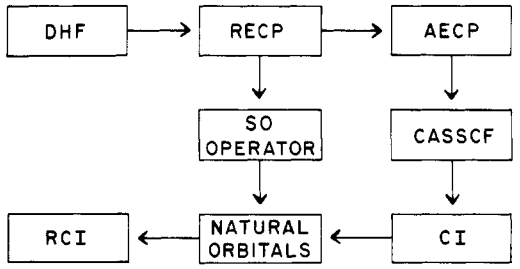

Figure 6. Schematic illustration of the relativistic CASSCF/CI/RCI method.

where U_{lj}s are lj-dependent radial numerical potentials and $|lmj\rangle$s are two-component Pauli spinors given by

$$|lmj\rangle = \begin{bmatrix} C(l^1/_2 j;m-^1/_2,^1/_2) & Y_{l,m-1/2} \\ C(l^1/_2 j;m+^1/_2,^1/_2) & Y_{l,m+1/2} \end{bmatrix} \quad (11)$$

in which $C(l^1/_2 j;m-^1/_2,^1/_2)$s are the Clebsch–Gordon coefficients. The summation over l actually should be up to ∞ in U^{REP}, although, in practice, this converges smoothly. The general rule is that L should be at least one higher than the maximum l value in the core.

In recent years Ermler, Christiansen, and co-workers[22-24] have generated RECPs for many elements in the periodic table. While numerical potentials of specific actinide and lanthanide elements such as U, Np, and Pu have been generated, published tables of RECPs derived from numerical DHF calculations of both actinide and lanthanide elements are not available at present. The numerical RECPs generated by these authors are fit into a convenient Gaussian form suggested by Kahn et al.[20] for molecular calculations. Rather than the Gaussian fits of RECPs themselves, tables of averaged ECPs (AECPs) and spin–orbit operators are more useful. When RECPs are averaged with respect to spin, they take a more convenient form suitable for polyatomic ab initio calculations.

The spin–orbit operator itself can be expressed in terms of RECPs as shown both by Hafner and Schwarz[87] and Ermler et al.[21] The radial part of the spin–orbit operator can be molded in a Gaussian analytical form convenient for use in molecular structure calculations. R. Pitzer has recently developed the codes to evaluate the spin–orbit integrals in a Gaussian basis set. The spin–orbit integrals thus obtained can be introduced either perturbatively or variationally. A first-order perturbation treatment of the spin–orbit coupling term is probably satisfactory for molecules containing the elements in the first two rows of the periodic table. For very heavy molecules, it is evident that the perturbative inclusion of the spin–orbit term is not accurate.

The present author[64] has developed an approach that takes advantage of recent advances in the nonrelativistic MCSCF/direct CI methods and incorporates all the relativistic effects, including the spin–orbit term. This method is delineated in Figure 6. The first section of this figure (DHF → RECP → AECP) is simply a schematic exemplification of the above description. Both relativistic and electron correlation effects tend to be large for clusters and molecules containing heavy-transition-metal and other main-group atoms. Averaged ECPs can be introduced into direct CI and MCSCF methods, in which electron correlation effects are taken into account to a high order, including all relativistic effects except spin–orbit coupling. In recent years we have employed the complete active space MCSCF method[102] (see Figure 6), abbreviated as CASSCF, for the generation of orbitals for the configuration interaction (CI) calculations. In this method a set of the most important electrons for chemical bonding (active electrons) are distributed in all possible ways among the orbitals referred to as the internal or active orbitals. The active orbitals are normally chosen as the set of orbitals that correlate into valence atomic orbitals at infinite separation of the various atoms in the molecule. The CASSCF method thus provides a zero-order ("valence") starting set of orbitals for the inclusion of higher order correlation effects.

The CASSCF method includes a full CI in the internal space. Thus, the number of configurations in the CASSCF can rise astronomically as more orbitals are included in the internal space. For example, a full CASSCF in the internal space of Zr_2 generates up to 15 000 configurations.[96] For the $^1\Sigma_g^+$ ground state of Mo_2 or W_2, we estimate that this number should be above 60 000 even when only the valence d and s orbitals are included. One method of bringing down the configuration count in the CASSCF appears to be the exclusion of some of the unimportant orbitals from the active space. This method has proved to be valuable where some of the antibonding type of orbitals are not very important in the bonding region although this technique is not size consistent if one needs to compare the molecular region with dissociation limits. Another method is to include very low lying orbitals in the core rather than in the active space. Relaxation of these core orbitals is allowed, although excitations of the electrons into these orbitals are not allowed. Yet another method of truncating the configurations in the MCSCF is to restrict the configurations by choosing a set of important reference configurations and then allowing single and double excitations from these. However, in the MCSCF this procedure is not often followed since one does not know a priori the list of important configurations for transition-metal compounds. Moreover, truncation of configurations using this procedure leads to a slower rate of convergence in the MCSCF in comparison to a full CASSCF.

Higher order electron correlation effects not included in the CASSCF are taken into account using the configuration interaction method. The CI calculations we have carried out are second-order CI (SOCI), MRSDCI (multireference single + double CI), first-order CI (FOCI), and POLCI. The first two methods are more accurate in comparison to the latter two methods. The SOCI calculations include (i) all configurations in the CASSCF, (ii) configurations generated by distributing $n - 1$ electrons in the internal space and one electron in the external space (n = number of active (valence) electrons), and (ii) configurations generated by distributing $n - 2$ electrons in the internal space and two electrons in the external space in all possible ways. The FOCI calculations include the first two sets of configurations described above for the SOCI calculations. The MRSDCI calculations include a subset of reference configurations in the SOCI determined by the most important configurations in the CASSCF (coefficient ≥ 0.07 or 0.05). Subsequently, single and double excitations from each of the reference configurations is allowed in the MRSDCI.

Large-scale CI calculations in recent years have been made possible with the advent of the graphical unitary group approach[85] (GUGA) and the Liu–Yoshimine symbolic CI method.[86] Schaefer and co-workers[85] have exploited the computational advantage of the unitary group method through loop-driven GUGA algorithms. Further ramifications of these methods and the coupled cluster methods can be found in the recent papers of Schaefer and co-workers.[97] The contracted CI (CCI) method of Siegbahn[103] is especially advantageous for carrying out CI calculations that contain several million configurations where this contraction does not lead to more than 2–5% error of the total uncontracted correlation energy. We have employed all of the above methods to obtain the electron correlation effects for molecules containing very heavy atoms. The electron correlation effects seem to be by far the most difficult effects to deal with even for very heavy molecules in comparison to relativistic and spin–orbit effects. Thus, the electron correlation problem still remains the bottleneck of accurate relativistic calculations. The largest CCI calculations done by our group to date included 2 million configurations on Pd_3[68] and 1.5 million configurations on Ag_3 and Au_3.

(102) Roos, B. *Adv. Chem. Phys.* **1987**, *67*, 399. Although the name CASSCF was suggested by Roos, Siegbahn, and co-workers, it appears that K. Ruedenberg and co-workers have used this technique before under a different name (fully optimized reaction space (FORS) MCSCF). See also: Schaefer, H. F.; Harris, F. E. *J. Chem. Phys.* **1968**, *48*, 4964.

(103) Siegbahn, P. E. M. *Int. J. Quantum Chem.* **1983**, *23*, 1870.

TABLE I: Reference Configurations Included in the RCI Calculations of Pd_3[a]

system	state	RCI reference configurations	
Pd_3	$^1A_2(A_2)$	$...5a_1^2 6a_1^2..3b_2^2 4b_2\alpha..2b_1^2 3b_1\beta..3a_2^2$	$^1A_2(A_2)$
		$...5a_1^2 6a_1^2..3b_2^2 4b_2\beta..2b_1^2 3b_1\alpha..3a_2^2$	
		$...5a_1^2 6a_1\alpha..3b_2^2 4b_2\alpha..3b_1^2..3a_2^2$	$^3B_2(A_2)$
		$...5a_1^2 6a_1\beta..3b_2^2 4b_2\beta..3b_2^2..3a_2^2$	
		$...4a_1^2 5a_1\alpha 6a_1\beta..4b_2^2..3b_1^2..3a_2^2$	$^3A_1(A_2)$
		$...4a_1^2 5a_1\beta 6a_1\alpha..4b_2^2..3b_1^2..3a_2^2$	
		$...4a_1^2 5a_1\alpha..4b_2^2..2b_1^2 3b_1\alpha..3a_2^2$	$^3B_1(A_2)$
		$...4a_1^2 5a_1\beta..4b_2^2..2b_1^2 3b_1\beta..3a_2^2$	
	$^3B_2(A_1)$	$...5a_1^2 6a_1\alpha..3b_2^2 4b_2\alpha..3b_1^2..3a_2^2$	$^3B_2(A_1)$
		$...5a_1^2 6a_1\beta...3b_2^2 4b_2\beta..3b_1^2..3a_2^2$	
		$...5a_1^2 6a_1\alpha..4b_2^2..3b_1^2..2a_2^2 3a_2\beta$	$^3A_2(A_1)$
		$...5a_1^2 6a_1\beta..4b_2^2..3b_1^2..2a_2^2 3a_2\alpha$	
		$...5a_1^2 6a_1\alpha..4b_2^2..2b_1^2 3b_1\alpha..3a_2^2$	$^3B_1(A_1)$
		$...5a_1^2 6a_1\beta..4b_2^2..2b_1^2 3b_1\beta..3a_2^2$	
		$...5a_1^2..4b_2^2..3b_1^2..3a_2^2$	$^1A_1(A_1)$

[a] We show only two states for Pd_3.

Relativistic CI (RCI) calculations are carried out following the CASSCF/CI methods (see Figure 6). The CASSCF/CI calculations described above include electron correlation corrections as accurately as possible but neglect the spin–orbit coupling term which is far from negligible for molecules containing heavy atoms. To illustrate, the $^3\Gamma_u(5_u)$–$^3\Gamma_u(3_u)$ spin–orbit splitting for Pt_2 is 15 600 cm^{-1}.[54] A RCI code for polyatomics[64] which yields spin–orbit corrections with an accuracy of 85–95% of the experimental values has been developed. In the RCI calculations spin–orbit integrals are obtained for Gaussian basis sets using R. Pitzer's modified ARGOS codes.[83] The spin–orbit integrals are transformed into the natural orbital basis obtained from CASSCF/CI and then added to the one-electron Hamiltonian matrix at the RCI step. Consequently, the spin–orbit coupling term is included variationally rather than perturbatively.

The RCI calculations in general include all configurations that mix in the presence of the spin–orbit coupling term as reference configurations. The inclusion of the spin–orbit coupling term in the Hamiltonian changes the normal point group symmetry of the molecule into the spin-double group. Thus, all configurations that have the same symmetry in the spin-double group could mix in the RCI. For a diatomic molecule all λ–s electronic states with the same Ω symmetry mix in the RCI. For example, $^1\Sigma_{0^+}^+$, $^3\Pi_{0^+}$, $^3\Sigma_{0^+}^-$, etc., could mix when the spin–orbit term is included.

The symmetry considerations for nonlinear polyatomic RCI calculations are best described by treating the spin functions in the double group of the molecular group and then multiplying the irreducible representations spanned by the spin functions with the spatial symmetry. The irreducible representations spanned by the various spin multiplets are obtained by correlating the three-dimensional rotation group representation $D^{(s)}$ ($s = 1$ for triplet) into the C_{2v}^2 group. For example, the triplet functions correlate into $A_2 + B_1 + B_2$ while the doublet spin functions correlate into E. Similarly, the quintet spin functions correlate into $2A_1 + A_2 + B_1 + B_2$.

Table I shows, as an example, the important reference configurations with appropriate spin combinations included in our earlier RCI calculations on Pd_3.[68] In general, all low-lying configurations of the same symmetry in the spin-double group of the molecular symmetry group should be included in the RCI calculations. For Pd_3 the $^1A_2(A_2)$ state could mix with $^3B_2(A_2)$, $^3A_1(A_2)$, and $^3B_1(A_2)$ states, where the label in the parentheses is the symmetry of the state in the C_{2v}^2 double group (the group of the Hamiltonian including spin–orbit coupling). The overall symmetry in the double group is simply the product of spatial symmetry and the symmetry of the spin functions. The RCI calculations of Au_3 included the two nearly degenerate $^2B_2$ and $^2A_1$ states with appropriate spins. Both these states correlate into the E representation in the C_{2v}^2 double group. Thus, the $^2B_2$ state (spin α) could mix with the $^2A_1$ state (spin β) and vice versa. Consequently, the RCI calculations of Au_3 included the important configurations for both these states with appropriate spins.

TABLE II: Comparison of Spectroscopic Properties of PdH with PtH

	R_e, Å		T_e, cm^{-1}		ω_e, cm^{-1}		D_e, eV	
state	PdH	PtH	PdH	PtH	PdH	PtH	PdH	PtH
$^2\Sigma_{1/2}^+$	1.53	1.59	0	1008	1948	2045	2.2	2.5
$^2\Delta_{5/2}$	1.59	1.61	3497	0	1817	2047	2.4	
$^3/_2$(I)	1.65	1.69	4599	2742	1711	2016	2.2	
$^3/_2$(II)	1.63		9362	27092	1721		1.7	
$^2\Pi_{1/2}$	1.67		9343	12818	1655		1.7	
$^2\Sigma^+$(II)	1.62		21904		1567			

Since the RCI codes developed up to now do not have the capabilities of direct CI procedures, these are restricted to calculations that include up to 20 000–30 000 configurations. The natural orbitals obtained from CASSCF/CI procedures can be partitioned into two external subsets based on density (occupancy) criterion. Those orbitals with occupancies less than a given threshold are grouped in the second set in this procedure. Thus the RCI calculations may be carried out in the internal and first subset of external orbitals. The evident advantage of this procedure is that it brings down the configuration count in the RCI to a manageable number for this code. However, the truncation of the orbitals and configuration in the RCI would lead to a higher energy in comparison to a more complete CASSCF/MRSDCI calculation. Thus RCI calculations are repeated with identical sets of configurations without the spin–orbit integrals. The differences in the energies and other properties obtained with and without the spin–orbit integrals then measure the effect of the spin–orbit term on these properties. The differences thus obtained in T_e, R_e, θ_e, and other properties are added as corrections to the CASSCF/MRSDCI results. Consequently, this procedure takes into account both electron correlation effects and spin–orbit effects.

III. Recent Applications of Relativistic Methods

In this section we describe and compare the importance of relativistic effects on electronic, spectroscopic, geometrical, and other properties of transition-metal clusters and hydrides. In addition, the impact of relativistic effects on the dipole moments and transition moments of main group IV hydrides and dihydrides are also considered. The emphasis is more on periodic trends within a group of the periodic table. Consequently, this section is not an overall review of all compounds in a class but portrays selected interesting comparisons of relativistic effects on the periodicities. The experimental techniques and experimental results on the investigations of transition metal clusters are described in ref 70–78.

A. Transition-Metal Hydrides (TMH). Two interesting comparisons of TMHs are PtH versus PdH and AuH vs AgH. The present author and co-workers[51] have completed relativistic calculations on PdH. Both ECP and all-electron calculations have been made by a number of other authors on AgH and AuH.[38-40] Wang and Pitzer[69] have carried out single-configuration SCF/RCI calculations on the low-lying electronic states of PtH. We use their results for PtH to compare the properties of PdH with PtH.

Table II compares the spectroscopic properties of PdH and PtH for the known states of PtH. As seen from Table II, the bond lengths of the electronic states of PtH do not increase much in comparison to PdH. This is not in accord with the expected trend as one goes down the periodic table which normally leads to longer bond lengths. Note that the $^2\Delta_{5/2}$ state of NiH has a bond length of 1.48 Å. Thus the $^2\Delta_{5/2}$ state of PtH should have a bond length of at least 1.7 Å in contrast with a bond length of 1.61 Å. For PtH, the analysis of the relativistic effects is complicated by the fact that the bond length is altered by both mass–velocity contraction and spin–orbit effects. The spin–orbit coupling can increase or decrease the bond lengths depending on what states mix in the RCI. The PtH molecule is considerably more stable in comparison to PdH. In fact, the ground state of the platinum atom is $^3D_3$ arising from $5d^96s^1$ while it is $^1S_0$ for Pd arising from

TABLE III: Comparison of Electronic States of AgH_2 with AuH_2

state	R_e, Å		θ, deg		E, eV	
	AgH_2	AuH_2	AgH_2	AuH_2	AgH_2	AuH_2
$^2B_2$	1.66	1.62	112	127	1.89	0.85
$^2\Sigma_u^+$	1.76	1.69	180	180	2.33	1.44
$^2\Sigma_g^+$	1.65	1.66	180	180	2.26	1.73
$M(^2S) + H_2$					0	0

the $4d^{10}$ configuration.[88] This interchange of the ground states of the two atoms seems to be primarily due to the relativistic stabilization of the 6s orbital of Pt which overcomes the enhanced stability attributed to the closed-shell d^{10} configuration. Consequently, the differences in the chemistry of Pt and Pd containing systems arise from this and the larger spin–orbit splitting in Pt in comparison to Pd.

The spin–orbit effects in PtH are so large in comparison to PdH that the energy separations of various states are quite different. For example, the ground state of PtH appears to be $^2\Delta_{5/2}$ while it is $^2\Sigma_{1/2}^+$ for PdH. The spin–orbit splittings of different states are substantially smaller for PdH in comparison to PtH.

The vibrational frequencies of the electronic states of PtH are larger compared to PdH contrary to the anticipated trend for a heavier diatomic. This evidently implies enhanced stability and deeper potential well for the electronic states of PtH in comparison to PdH attributed to larger relativistic effects of PtH.

The bond lengths of the $^1\Sigma^+$ ground states of AgH and AuH derived from RECP SCF calculations are 1.70 and 1.59 Å, respectively.[40] The corresponding ω_e values are 1537 and 2029 cm^{-1}, respectively. Thus, it is evident that the relativistic mass–velocity contraction has a considerable influence on the R_e and ω_e values of these two species. A comparison of nonrelativistic ECP and RECP SCF calculations on these two species reveals that relativistic effects contract the R_e of AuH by 0.23 Å compared to a contraction of only 0.06 Å for AgH.

B. Transition-Metal Dihydrides. In this section we compare the properties of AgH_2 with AuH_2[56,67] and PtH_2[50] with PdH_2.[60] Table III shows the properties of the electronic states of AgH_2 and AuH_2 obtained by using comparable CASSCF/CI calculations which include excitations from the d shells of the metal atom. The calculated bending potential energy surfaces of the two species are compared in Figure 7. As seen from Table III, AuH_2 is about 1 eV more stable than AgH_2 in comparison to $M + H_2$. This stabilization is once again brought about by relativistic effects. In comparing the M–H bond lengths of the two species, we find that they decrease for the $^2B_2$ and $^2\Sigma_u^+$ states while they are almost the same for $^2\Sigma_g^+$. This trend is consistent with the observed trend for MH. The bond angle in the $^2B_2$ state is larger for AuH_2 mainly because the metal–H bonding is stronger in AuH_2.

As seen from Figure 7, the $^2B_2$ surface of AgH_2 contains double bent minima while the first small-angle minimum is absent for AuH_2. This minimum is attributed to a weak $Ag(^2P)$ H_2 complex. The ^2S–$^2P_{1/2}$ splittings of gold and silver are 40 000 and 30 000 cm^{-1}, respectively. Since $Ag(^2P)$ is much lower in energy, it forms a weak complex with H_2. The Au–H bonds were found to be more ionic. A comparison of the Mulliken populations of the two species revealed that the M(p) populations are much larger for Ag while the M(s) populations are larger for Au, confirming the stabilization of the 6s orbital of gold.

Table IV compares the electronic states of PtH_2 with the corresponding states of PdH_2. Figure 8 compares the bending potential energy surfaces of PtH_2 and PdH_2 obtained by using the CASSCF method. As seen from Table IV, the PtH bond lengths are shorter than the PdH bond lengths for most of the states. The $^1A_1$ PtH_2 bent minimum is much more stable than the corresponding minimum of PdH_2. This is primarily because the ground state of Pd arises from the $4d^{10}$ configuration while the ground state of Pt is $5d^96s^1$ ($^3D_3$). The ^1S state arising from d^{10} is not likely to form a strong bond with H_2 unless excitations into the s shell are favorable. The 5d–6s excitation energy for Pt is considerably smaller than the 4d–5s excitation energy of the palladium atom. These are the reasons for the difference in the properties of PtH_2 and PdH_2.

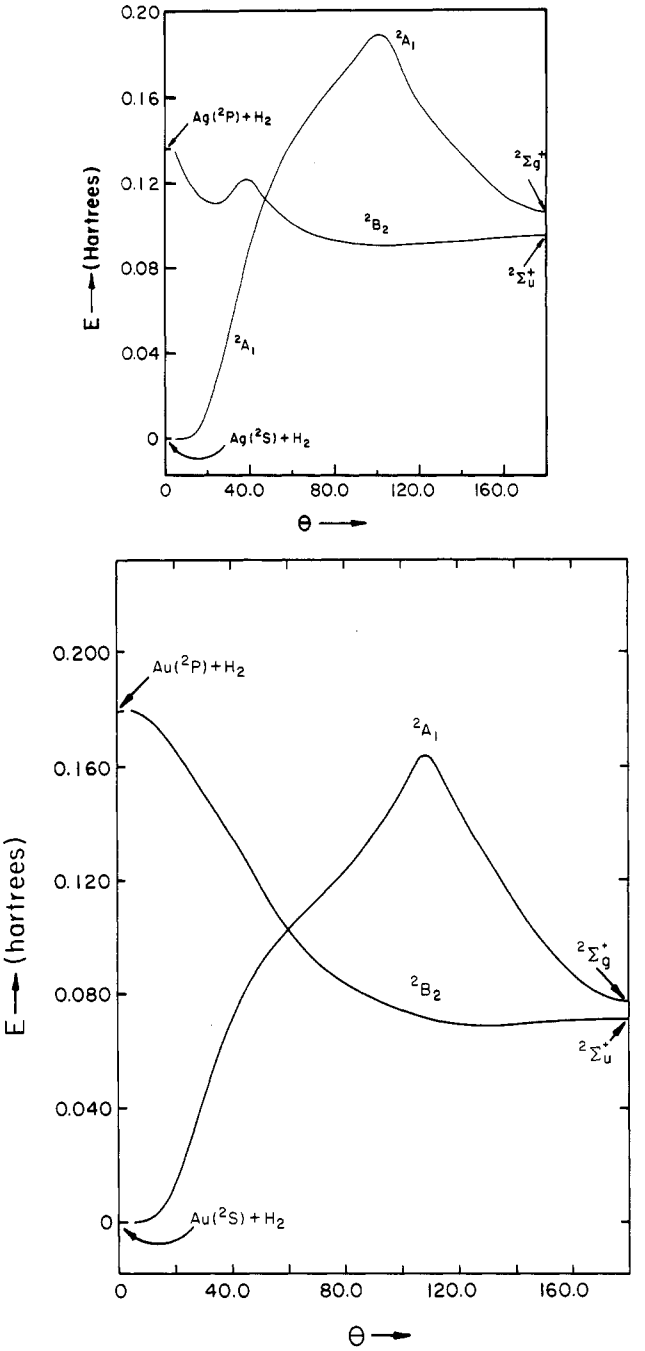

Figure 7. Bending potential energy curves for AgH_2 (top) and AuH_2 (bottom).

TABLE IV: Comparison of the Low-Lying Electronic States of PtH_2 and PdH_2

state	PtH_2			PdH_2		
	r_e, Å	θ_e, deg	E, eV	r_e, Å	θ_e, deg	E, eV
$^1A_1$	1.52	85.1	0.0	1.67	30	0.0
$^1A_1$				1.50	62	0.25
$^1\Sigma_g^+$	1.68	180	2.33	1.62	180	2.10
$^3\Delta_g$	1.70	180	2.01	1.65	180	2.93
$^3\Pi_g$	1.71	180	3.0	1.68	180	3.55
$^1\Pi_g$	1.71	180	3.02	1.69	180	3.70
$^1\Delta_g$	1.69	180	4.98	1.79	180	4.63

As seen from Figure 8, both $Pd(^1S_0)$ and $Pt(^1S_0)$ insert into H_2 spontaneously while the $^3D_3$ atoms have to surmount large barriers for insertion into the hydrogen bond. Poulin et al.[104] also came to the same conclusion using a SCF/variational–pertur-

(104) Poulin, E.; Garcia-Prieto, J.; Ruiz, M. E.; Novaro, O. *Int. J. Quantum Chem.* **1986**, *24*, 1181.

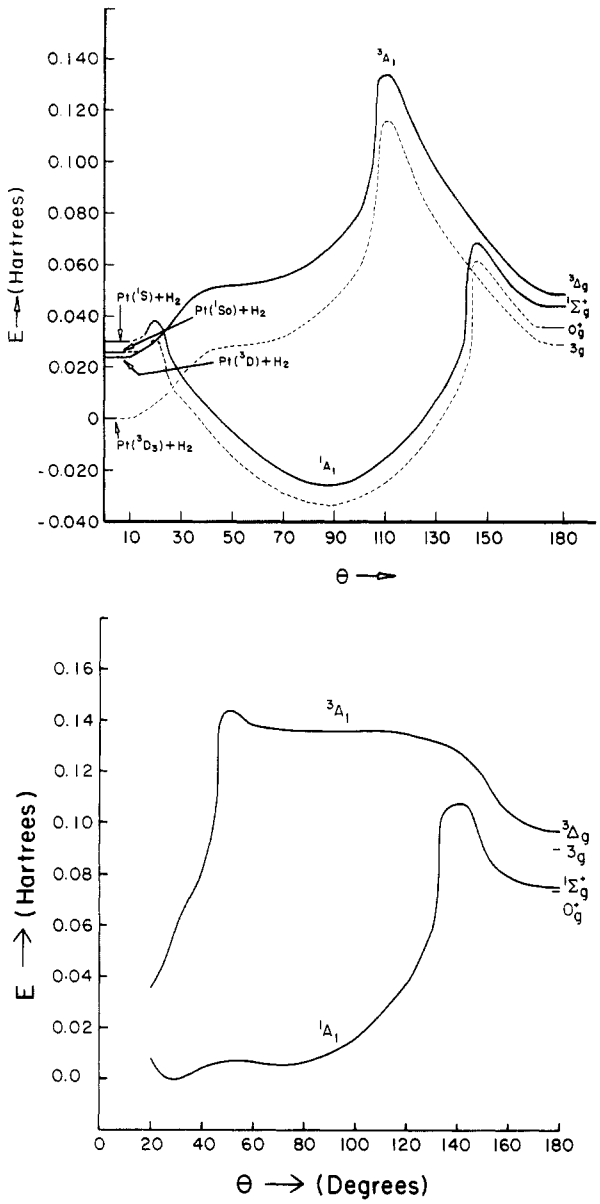

Figure 8. Comparison of the bending potential energy surfaces of the triplet and singlet states of PtH_2 (top) and PdH_2 (bottom).

bational CI method on PtH_2. Low and Goddard[105] also found that $Pt(^1S_0)$ inserts into H_2 spontaneously. There are many differences in the potential energy surfaces of the two species due to relativistic effects.

The PdH_2 $^1A_1$ surface contains a weak complex of $Pd(d^{10})H_2$ followed by a second bent minimum which arises from the relativistic stabilization of the 4d–5s excitation (Figure 8). In fact, nonrelativistic calculations on PdH_2 such as the one made by Blomberg et al.[98] do not yield the second bent minimum. However, the relativistic GVB/CI calculations of Low and Goddard[99] on the $^1A_1$ state of PdH_2 yield this minimum. The relativistic spin–orbit effects are considerably larger for PtH_2 than PdH_2 (see Figure 8). For example, the $^3\Pi_g$ spin–orbit splittings for PtH_2 and PdH_2 are 0.74 and 0.18 eV, respectively. More detailed discussions on other transition-metal dihydrides such as CoH_2, ScH_2, RhH_2, YH_2, NbH_2, etc., can be found in ref 48, 59, 63, 65, and 100.

C. Transition-Metal Dimers. Our group has completed calculations on many electronic states of Pt_2,[54] Pd_2,[64] and Rh_2[91] and the ground states of Ag_2 and Au_2.[66] A critical comparison of the spectroscopic properties of some of these dimers and a comprehension of the impact of relativity on these properties seem to be quite valuable. Tables V and VI show the calculated spectroscopic properties of some of the low-lying electronic states of Pt_2 and Pd_2, respectively. For Pd_2 we have calculated the spectroscopic properties of 41 electronic states (ref 64). In Table VI only some of these are shown. In comparing the spectroscopic properties of these two species, we note that the bond lengths of the various states of Pt_2 are much shorter than the corresponding bond lengths in Pd_2. A dramatic contrast is in the $^1\Sigma_g^+$ state of the two dimers. For Pt_2 this arises predominantly from the π_g^2 configuration with a bond length of 2.45 Å while for Pd_2 it arises predominantly from the $1\sigma_u^2$ configuration with a bond length of 2.87 Å where we show only the highest occupied orbital. This is consequence of the fact that the ground state of Pt is $5d^96s^1$ ($^3D_3$) while the corresponding ground state of Pd is $4d^{10}$ ($^1S_0$). The switching of the two states is brought about by the relativistic stabilization of the 6s orbital of Pt as noted before.

The spin–orbit splittings of Pd_2 and Pt_2 for a selected state are compared in Figure 9. As seen in Figure 9, the $^3\Gamma_u(5_u)$–$^3\Gamma_u(3_u)$

TABLE V: Spectroscopic Properties of Pt_2

state	R_e, Å	T_e, cm^{-1}	ω_e, cm^{-1}
$\delta_u^2\,^3\Sigma_g^-(0_g^+)$	2.456	0.0	189
$\delta_u^3\delta_g^3\,^3\Gamma_u(5_u)$	2.570	614	193
$\delta_u^3\pi_g^3\,^3\Phi_u(4_u)$	2.580	1074	240
$\pi_g^2\,^3\Sigma_g^-(0_g^+)$	2.423	3064	215
$\sigma_u\pi_g^3\,^3\Pi_u(2_u)$	2.396	3214	306
$\sigma_u\pi_g^3\,^3\Pi_u(1_u)$	2.398	3556	305
$\sigma_u\delta_u^3\,^3\Delta_g(2_g)$	2.493	5838	202
$\pi_g^2\,^3\Sigma_g^-(1_g)$	2.428	5935	219
$\sigma_u\pi_g^3\,^3\Pi_u(0_u^-)$	2.400	7500	304
$\sigma_u\pi_g^3\,^3\Pi_u(0_u^+)$	2.400	7501	304
$\delta_u^2\,^1\Gamma_g(4_g)$	2.558	7886	196
$\sigma_u\delta_u^3\,^3\Delta_g(3_g)$	2.485	8164	208
$\delta_u^3\delta_g^3\,^3\Sigma_u^+(1_u)$	2.578	8180	191
$\delta_u^3\delta_g^3\,^3\Gamma_u(4_u)$	2.570	8259	192
$\delta_u^2\,^3\Sigma_g^-(1_g)$	2.459	8282	175
$\delta_u^3\delta_g^3\,^3\Sigma_u^+(0_u^-)$	2.578	8755	188
$\sigma_u\pi_g^3\,^1\Pi_u(1_u)$	2.455	9556	197
$\pi_g^2\,^1\Sigma_g^+(0_g^+)$	2.453	9765	180
$\sigma_u\delta_u^3\,^3\Delta_g(1_g)$	2.487	10810	206
$\sigma_u\delta_u^3\,^1\Delta_g(2_g)$	2.539	11286	170
$\delta_u^3\pi_g^3\,^3\Pi_u(3_u)$	2.553	15234	277
$\delta_u^3\delta_g^3\,^3\Gamma_u(3_u)$	2.571	15806	191

TABLE VI: Spectroscopic (MRSDCI/RCI) Properties of Some of the Electronic States of Pd_2

state	R_e, Å	T_e, cm^{-1}	ω_e, cm^{-1}
$^3\Sigma_u^+(1_u)$	2.48	0	159
$^3\Sigma_u^+(0_u^-)$	2.48	9	161
$^3\Sigma_u^+$	2.48	214	160
$^1\Sigma_g^+(0_g^+)$	2.87	1257	121
$^1\Sigma_g^+$	2.87	1328	121
$^3\Pi_g(1_g)$	2.55	1649	160
$^3\Pi_g(0_g^+)$	2.58	1770	159
$^3\Pi_g$	2.55	1888	160
$^3\Pi_g(0_g^-)$	2.55	2531	160
$^3\Delta_g(2_g)$	2.53	2575	173
$^3\Delta_g(3_g)$	2.55	2629	169
$^3\Delta_u(3_u)$	2.62	2679	154
$^3\Delta_u(2_u)$	2.62	2825	159
$^3\Pi_u(2_u)$	2.51	3075	175
$^3\Pi_u(1_u)$	2.50	3356	176
$^1\Pi_g$	2.50	3536	162
$^3\Delta_g$	2.55	3718	169
$^1\Pi_g(1_g)$	2.50	3787	161
$^3\Delta_u$	2.62	3905	154
$^3\Pi_u$	2.51	3930	175
$^1\Delta_g$	2.64	3948	151
$^1\Delta_u$	2.61	3991	188
$^3\Pi_u(0_u^-)$	2.53	4052	179

(105) Low, J. J.; Goddard III, W. A. *Organometallics* **1986**, *5*, 609.

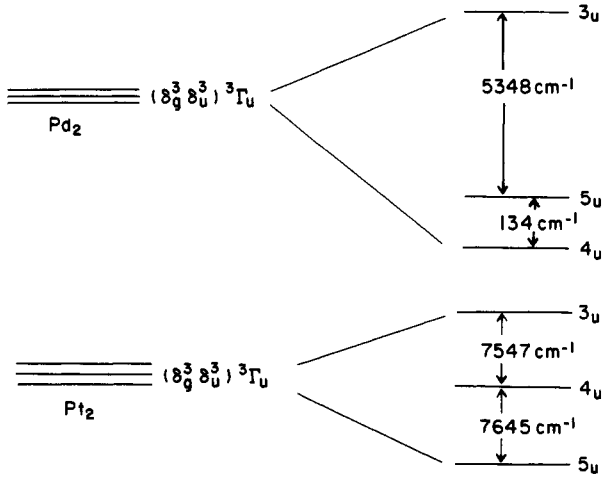

Figure 9. Spin–orbit splitting of $^3\Gamma_u(\delta_g^3\delta_u^3)$ states of Pt_2 and Pd_2.

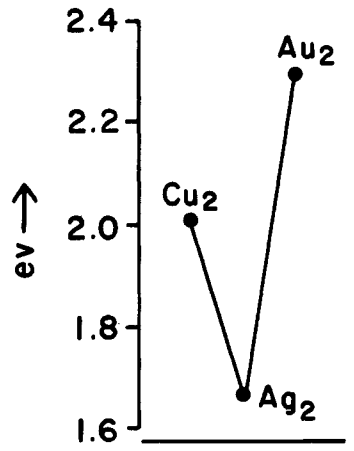

Figure 10. D_es of Cu_2, Ag_2, and Au_2.

splitting for Pt_2[54] is 15 192 cm^{-1} compared to 5214 cm^{-1} for Pd_2.[64] Thus, the spin–orbit effects are magnitudes larger for Pt_2. In addition, the spin–orbit coupling term mixes states of different symmetry that do not mix otherwise. For example, the 0_g^+ state of Pt_2 is 32% $^3\Sigma_g^-(\delta_u^2)$, 30% $^1\Sigma_g^+(\delta_u^2)$, 17% $^1\Sigma_g^+(\delta_g^2)$, and 15% $^3\Sigma_g^-(\delta_g^2)$.

The ω_e values are surprisingly larger for the electronic states of Pt_2 than the corresponding states of Pd_2. Although, the effective mass of Pt_2 would be much larger, the potential wells of the various electronic states are much deeper yielding larger ω_es for Pt_2. Taylor et al.[70] have recently confirmed our predictions on the electronic states of Pt_2[54] using jet-cooled resonant two-photon spectroscopy of Pt_2. These authors also recalculated the thermodynamic $D_0^0(Pt_2)$ using the partition function obtained from the theoretical energy separations. The $D_0^0(Pt_2)$ obtained this way was found to be in excellent agreement with a direct spectroscopic value obtained by Taylor et al.[70]

Comparison of the coinage metal dimers, namely, Cu_2, Ag_2, and Au_2, appears to provide a very good basis for understanding of relativistic effects. We carried out CASSCF/MRSDCI calculations which included up to 80 000 configurations on Ag_2 and Au_2. The SCF/SDCI method was used by Walch et al.[72] to study the ground state of Cu_2. Figure 10 shows the plot of the D_es of these three species in the $^1\Sigma_g^+$ ground state to demonstrate the influence of relativity on the periodicities of these systems. As seen from this figure, Au_2 is an "anomaly" in that it has an unusually large D_e in the triad. Note that the gold dimer has also a much shorter bond length in comparison to Ag_2.

Table VII shows the CASSCF/CI/RCI spectroscopic properties of some of the 36 electronic states of Rh_2 calculated before.[91] As seen from this table, the Rh–Rh bond lengths are substantially shorter for the various states in comparison to the neighboring dimer (Pd_2). This is mainly due to enhanced bonding in Rh_2 and

TABLE VII: Spectroscopic Properties of Some of the Low-Lying States of Rh_2 Including Spin–Orbit Effects

state	R_e, Å	T_e, cm^{-1}	ω_e, cm^{-1}
$^5\Delta_g(4_g)$	2.26	0.0	305
$^5\Delta_g(3_g)$	2.28	336	265
$^5\Delta_g(2_g)$	2.26	886	279
$^5\Delta_g$	2.28	1192	266
$^1\Gamma_g(4_g)$	2.53	6056	164
$^1\Gamma_u(4_u)$	2.55	6177	176
$^3\Sigma_g^-(0_g^+)$	2.54	6457	165
$^3\Sigma_g^-(1_g)$	2.54	6461	165
$^3\Gamma_u(4_u)$	2.57	6573	182
$^3\Gamma_u(3_u)$	2.57	6573	182
$^3\Delta_g(2_g)$	2.35	6662	231
$^3\Delta_g(1_g)$	2.36	6890	231
$^3\Delta_g(3_g)$	2.36	6892	232
$^1\Pi_u$	2.54	7094	148
$^1\Pi_g(1_g)$	2.58	7616	176
$^5\Sigma_g^+(2_g)$	2.36	7964	313
$^5\Sigma_g^+(1_g)$	2.36	7964	313
$^5\Sigma_g^+(0_g^+)$	2.36	7964	313
$^3\Pi_g(2_g)$	2.31	8457	321
$^1\Delta_u(2_u)$	2.60	8459	186
$^3\Pi_u(1_u)$	2.31	8992	234

TABLE VIII: Energy Separations of the Electronic States of Ag_3 and Au_3 Including the Spin–Orbit Effects[a]

state	R_e, Å	θ_e, deg	E, kcal/mol
Au_3 $^2B_2\alpha$	2.60	65.7	0
Au_3 $^2A_1\alpha$	2.72	56.4	0.16 (0.23)
Ag_3 $^2B_2\alpha$	2.72	63.7	0
Ag_3 $^2A_1\alpha$	2.88	54.2	0.69

[a] Number in parentheses includes Davidson's correction.

multiple bonding in some of the states. The ground state of atomic Rh ($4d^85s^1$) facilitates considerable 5s–5s bonding in addition to partial 4d–4d bonding. The spin–orbit effects are also found to be nonnegligible for the electronic states of Rh_2. For example, the $^5\Delta_g(4_g)$–$^5\Delta_g(2_g)$ splitting is 886 cm^{-1}.

The analysis of the weights of the various configurations in the CI wave functions of the electronic states of Rh_2 showed that the weights of the leading configurations for most of the electronic states is less than 40%.[91] This evidently demonstrates the need for a MCSCF/CI treatment for such dimers. The only states with weights between 54 and 63% are $^5\Delta_g$, $^1\Gamma_u$, $^3\Delta_g$, $^5\Sigma_g^+$, $^3\Delta_g$(II), $^3\Gamma_g$, $^5\Gamma_g$, and $^3\Pi_g$. The general trend is that low-Γ states tend to be mixtures of many electronic configurations while the high-Γ states are a bit purer.

It is of interest to compare the properties of Rh_2 with the lighter dimer in that group, namely, Co_2. Shim and Gingerich[93] have carried out all-electron SCF/valence CI calculations on Co_2. Using their theoretical calculations, these authors recalculated the third-law D_0^0 value as 0.95 ± 0.26 eV. This, however, contradicts another third-law D_0^0 value of 1.69 eV obtained by Kant and Strauss.[94] In any event, it is evident that the Co_2 dimer is more weakly bound in comparison to Rh_2 ($D_0(Rh_2) \sim 2.9$ eV). The ground state of Co_2[93] was found to be $^5\Sigma_g^+$ at the SCF/valence CI level of theory which is not reliable for predicting the energy separations or the ground state of transition metal dimers. However, even raw data are scarce for transition-metal dimers. The R_e and ω_e values of the ground-state Co_2 obtained in ref 93 are 2.56 Å and 162 cm^{-1}. In comparing these properties with Rh_2, we find that Rh_2 has a much shorter bond length (R_e = 2.26 Å, ω_e = 305 cm^{-1} for $^5\Delta_g$) and larger vibrational frequency. The larger D_0^0 of Rh_2 is also consistent with this.

D. Transition-Metal Trimers. Relativistic MCSCF/CI/RCI calculations have been completed on some heavy-transition-metal trimers such as Pd_3,[68] Ag_3, and Au_3.[49,66] Walch et al.[72] have carried out SCF/SDCI/coupled pair formalism (CPF) calculations on Cu_3 and Ag_3. We briefly summarize the importance of relativistic effects in these compounds. A more complete review of coinage metal clusters can be found in ref 106.

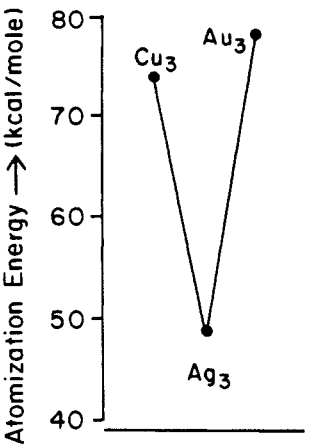

Figure 11. AEs of Cu_3, Ag_3, and Au_3.

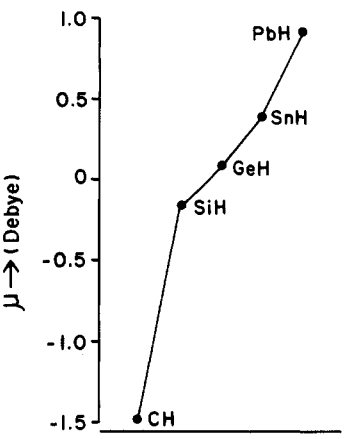

Figure 12. Dipole moments of CH–PbH.

The geometries and energy separations obtained by using CASSCF/MRSDCI calculations which included all 33 electrons and up to 421 000 configurations are shown in Table VIII for both Ag_3 and Au_3. As seen from this table, both Ag_3 and Au_3 have two nearly degenerate states of $^2B_2$ and $^2A_1$ symmetry with isosceles triangular geometry. These two states are the Jahn–Teller components of the same $^2E'$ state with equilateral triangular geometry. The geometries of both the states are acute triangles with energy splittings of less than 1 kcal/mol.

A full MRSDCI calculation that included all 33 electrons and 1.5 million configurations was carried out on both Ag_3 and Au_3 with the objective of calculating the atomization energies (AE) for the two clusters. The AEs of the two clusters are defined as the energies required for the process

$$M_3(^2B_2) \rightarrow 3M(^2S)$$

The AE was found to be 76 kcal/mol for Au_3 in comparison to an experimental value of 88 kcal/mol obtained by Hilpert and Gingerich.[95] The corresponding AE for Ag_3 is 48 kcal/mol including Davidson's correction. The Au–Au bond lengths are also much shorter than the Ag–Ag bond lengths due to relativistic effects in all states.

Figure 11 compares the atomization energies of Cu_3, Ag_3, and Au_3. The AE of Cu_3 in that figure is from Walch et al.'s work. As seen from this figure, the AE decreases in moving from Cu to Ag but increases dramatically for Au_3, even surpassing the AE of Cu_3. Thus, the gold anomaly noticed in the dimers is evident in the AEs and the geometries of the trimers, too.

The spin–orbit effects were found to be very significant for Au_3. When spin–orbit coupling is included, the $^2B_2$ electronic state (spin α) mixes with the $^2A_1$ state (spin β) and vice versa. The ground state of Au_3 is found to be 93% $^2B_2$ and 0.6% $^2A_1$. The nearly degenerate $^2A_1$ state actually consists of 92% $^2A_1$ and 1% $^2B_2$.

We have recently completed CASSCF/MRSDCI calculations on 10 electronic states of Pd_3[68] which included up to 2 million configurations. In addition, the effect of the spin–orbit term was investigated by using the RCI method. The final CASSCF/MRSDCI/RCI geometries and energy separations of 21 electronic states are shown in Table IX.

The overall theoretical energy separations of the various electronic states found for Pd_3 are in accord with the observed photoelectron spectrum of Pd_3^-.[71] The photoelectron spectrum of Pd_3^- is quite complex and contained some 16 peaks labeled A–P. These peaks are quite closely placed in the spectrum in agreement with the theoretical energy level separations (Table IX). It is evident that some of these very closely spaced peaks are due to the spin–orbit components of the various states of Pd_3. The A–P splitting of the experimental spectrum is about 0.6 eV, indicating there are at least 16 states below 0.6 eV of the ground state of Pd_3. As can be seen from table IX, our calculations are in full agreement with this, although this table is not exhaustive.

TABLE IX: The Electronic States of Pd_3

state	R_e, Å	θ_e, deg	E, eV
$^1A_2(A_2)$	2.67	55	0.0
$^1A_2$	2.67	55	0.03
$^3B_2(B_1)$	2.52	67.5	0.308
$^3B_2(A_1)$	2.52	67.5	0.309
$^3B_2(A_2)$	2.52	67.5	0.319
$^3B_2$	2.52	67.5	0.31
$^3A_2(A_1)$	2.64	67.8	0.339
$^3A_1(B_2)$	2.60	70	0.345
$^3A_1(B_1)$	2.60	70	0.345
$^3A_1(A_2)$	2.60	70	0.348
$^3A_1$	2.60	70	0.35
$^3A_2(B_1)$	2.64	67.8	0.354
$^3A_2(B_2)$	2.64	67.8	0.36
$^3A_2(A_1)$	2.64	67.8	0.36
$^1A_1$	2.90	60	0.41
$^3B_1(B_2)$	2.60	65	0.438
$^3B_1(A_2)$	2.60	65	0.444
$^3B_1(A_1)$	2.60	65	0.45
$^3B_1$	2.60	65	0.45
$^5A_2$	2.77	57	1.07
$^5B_1$	2.67	82	2.13

The Mulliken population analyses of the various electronic states of Pd_3 revealed considerable $4d^95s^1$–$4d^{10}$ mixing in most of the electronic states since the gross metal d populations are between 9.4 and 9.5 per atom. The quintet electronic states were found to be somewhat purer.

The calculated atomization energy of Pd_3 with respect to the three $Pd(^3D)$ atoms is 124 kcal/mol including Davidson's correction. The dimer was found to have a D_e of 48 kcal/mol with respect to $Pd(^3D)$ at the same level of theory. Thus Pd_3 is found to be substantially more stable in comparison to the dimer.

E. Relativistic Effects on Dipole Moments and Transition Moments. The influence of relativity on one-electron properties such as dipole and transition moments of the electronic states has been studied recently following the development of codes to calculate the dipole and transition moments from RCI wave functions.[52,57,62] These codes have now been applied successfully to many main-group heavy hydrides and dihydrides.

The dipole and transition moments of heavy group IV hydrides have received considerable attention in recent years. There is some controversy in the literature on the dipole moment of GeH. An experimental value of 1.24 ± 0.1 D obtained by Brown and coworkers[79] has been seriously questioned by several theoretical calculations, all of which converge near 0.09 D.[57,80–82] The smaller value of the dipole moment of GeH is also supported by electronegativity arguments.

Figure 12 shows the relative trends of the dipole moments of CH–PbH. The dipole moments of SnH and PbH were calculated by the present author and co-workers[57] for the first time using the RCI method including the spin–orbit term. As seen from this figure, the dipole moment of GeH is expected to be close to zero

(106) Balasubramanian, K. *J. Mol. Struct. (THEOCHEM)*, in press.

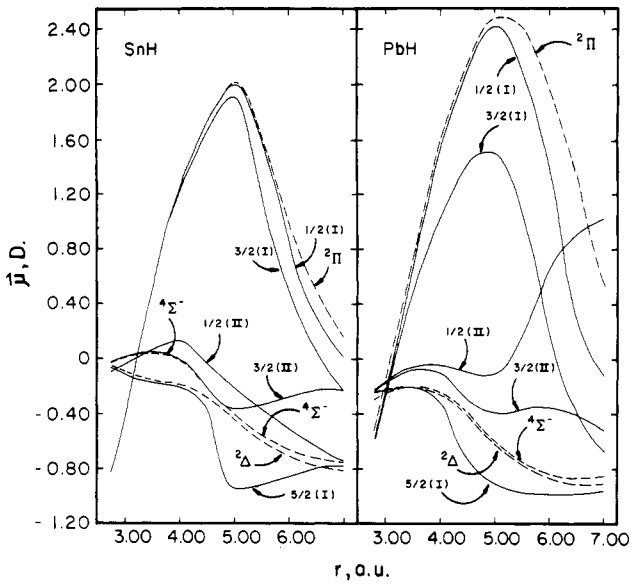

Figure 13. Transition moments of electronic transitions for SnH and PbH.

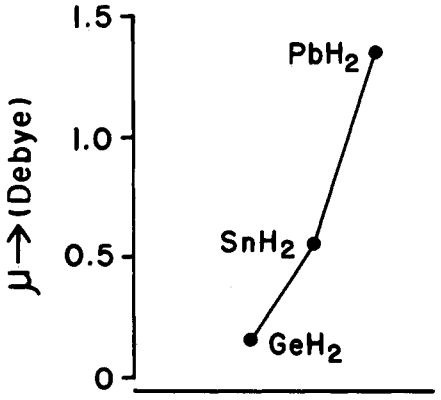

Figure 14. Dipole moments of GeH_2–PbH_2 in the $^1A_1$ state.

since the dipole moment of SiH is negative while the dipole moment of SnH is positive. Thus GeH is the transition point between nonmetallic and metallic characters in that group. The dipole moment of PbH is considerably larger as seen by comparing the slopes of GeH–SnH and SnH–PbH curves. This upward shift in the slope is primarily due to relativistic effects considering the fact that SiH, GeH, and SnH are almost collinear in Figure 12.

The comparison of the transition moments of SnH and PbH is also of considerable interest. Figure 13 shows the transition moments for some electronic transitions of the two species as a function of internuclear distance. Note the sharp increase in the transition moment of the $^1/_2(I) \rightarrow {}^1/_2(II)$ ($^2\Pi_{1/2}$–$^4\Sigma_{1/2}$) transition for PbH. In the same way the transition probability of the $^3/_2(I) \rightarrow {}^3/_2(II)$ ($^2\Pi_{3/2} \rightarrow {}^4\Sigma^-_{3/2}$) transition is also increased substantially for PbH. This increase in the transition moments for PbH is brought about primarily through relativistic spin–orbit contamination of different electronic states that do not mix in the absence of spin–orbit coupling. Note that both the transitions are spin-forbidden in the absence of the spin–orbit term since they correspond to a $^4\Sigma^-$–$^2\Pi$ transition. This becomes allowed due to relativistic effects since the $^1/_2$ state is a mixture of $^4\Sigma^-_{1/2}$ and $^2\Pi_{1/2}$. Similarly, the $^3/_2$ state is a mixture of $^2\Pi_{3/2}$ and $^4\Sigma^-_{3/2}$. This mixing is larger for PbH, resulting in larger transition moments for PbH.

Figure 14 shows the dipole moments of GeH_2, SnH_2, and PbH_2 in the $^1A_1$ state obtained recently by the present author.[62] Although, the dipole moment of PbH_2 should not be considered very accurate since it does not include the effect of the spin–orbit term, the observed trend for GeH, SnH, and PbH dipole moments is also seen in GeH_2–PbH_2. Note the upward tilt in the SnH_2–PbH_2 curve in comparison to GeH_2–SnH_2 curve. This tilt is once again a manifestation of large relativistic effects in PbH_2.

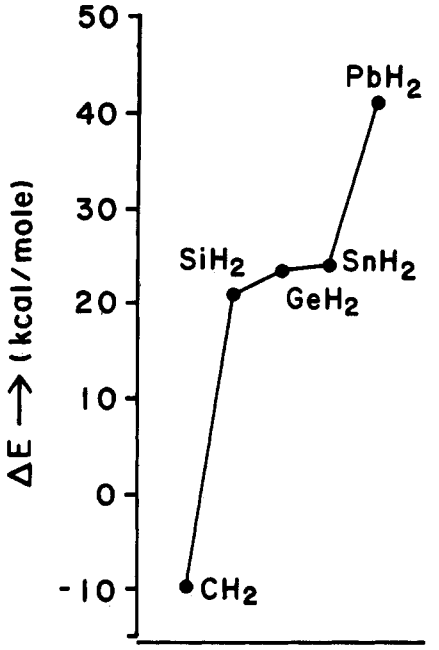

Figure 15. Comparison of $^1A_1$–$^3B_1$ splittings for CH_2–PbH_2.

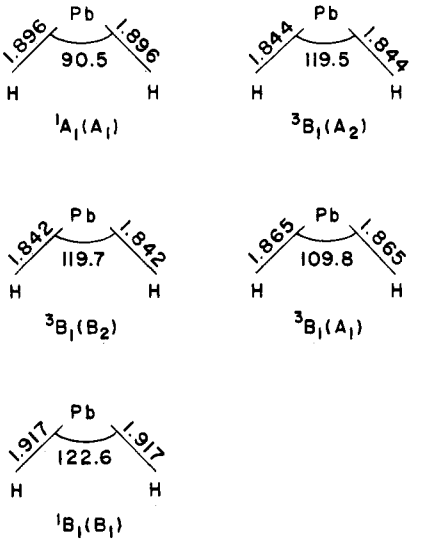

Figure 16. Geometries of the electronic states of PbH_2. Note the dramatic change in the geometry of the $^3B_1(A_1)$ component due to relativistic effects.

In recent years the singlet–triplet energy separations of the group IV dihydrides have been the topics of many investigations (see ref 62 for a brief review). The lightest analogue of these, namely, CH_2, has a $^3B_1$ bent ground state while all the heavier species have $^1A_1$ ground states. Figure 15 shows the $^1A_1$–$^3B_1$ splittings for CH_2–PbH_2. The $^1A_1$–$^3B_1$ splittings in this figure for GeH_2, SnH_2, and PbH_2 were obtained recently by the current author.[62] Note that these splittings are within 4 kcal/mol for SiH_2–SnH_2, while they dramatically increase to 42 kcal/mol for PbH_2. This is another manifestation of the so-called "inert pair" effect which is actually due to the relativistic stabilization of the $6s^2$ shell in Pb which leads to a substantially larger $^1A_1$–$^3B_1$ splitting for PbH_2.

The spin–orbit term has a large impact on the geometries of the electronic states of PbH_2. Figure 16 shows the geometries of the low-lying electronic states of PbH_2. As seen from this figure, the H–Pb–H bond angle of the $^3B_1(A_1)$ component decreases by almost 10° as a consequence of large spin–orbit coupling of the lead atom. This change is brought about primarily by the mixing of $^3B_1(A_1)$ with the $^1A_1(A_1)$ ground state of PbH_2. The analysis of the RCI wave functions reveals that this state is actually 67% $^3B_1(A_1)$ and 24% $^1A_1(A_1)$ (ground state). Consequently, spin–orbit

effects make significant impact not only on the electronic energy levels but also on the geometries of molecules containing heavy atoms.

IV. Conclusion

In this article we reviewed the recent developments in relativistic quantum mechanical methods and their applications to some transition-metal and main-group compounds. Special emphasis was placed on the impact of relativity on the periodic trends of molecules within certain groups of the periodic table. The anomalies in the trends for the very heavy molecules were explained.

Acknowledgment. Most of the research described here was supported by the Office of Basic Energy Sciences, Chemical Science Division of the U.S. Department of Energy under Grant DE-FG02-86ER13558. The main group research was supported by National Science Foundation Grant CHE 8520556. I express special thanks and gratitude to Professor Kenneth S. Pitzer, who motivated me and provided constant encouragement all these years to pursue relativistic quantum chemistry. I also thank my coworkers Prof. Sheng H. Lin and Drs. Douglas Chapman, M. Z. Liao, P. Y. Feng, and C. Ravimohan.

ARTICLES

A MO-CI Study on the Interaction of Copper(I) with Methylene: The $(CuCH_2)^+$ Carbene-like Ground State

J. Planelles,† M. Merchán, I. Nebot-Gil, and F. Tomás*

Departament de Química-Física, Facultat de Química, Universitat de València, Dr. Moliner 50, Burjassot, 46100 València, Spain *(Received: May 18, 1988; In Final Form: April 13, 1989)*

MO-CI calculations of the low-lying states of the $(CuCH_2)^+$ complex have been carried out using the multireference CIPSI algorithm. Special attention has been paid to build an adequate monoelectronic basis set for CI step. A $^1A_1$ ground state has been found, formed by the interaction between ^1S Cu^+ and $^1A_1$ CH_2, showing a binding energy about 57 kcal mol^{-1}.

I. Introduction

The interaction of a transition metal with methylene is currently receiving growing attention mainly for the following reasons: (i) synthesis and characterization of transition-metal methylene complexes is of special interest in organometallic chemistry;[1] (ii) metal complexes containing CH_2 ligands are proposed as intermediates in many homogeneous and heterogeneous catalytic reactions of considerable practical interest;[2] (iii) reliable theoretical studies may play a relevant role in understanding the common features and relationships between organometallic chemistry, surface chemistry, and catalysis, areas that are closely related.[3]

During the past few years, great efforts have been devoted to the study of transition-metal–methylene bonding from both experimental and theoretical points of view. Experimental bond dissociation energies for gas-phase transition-metal–methylene molecular ions, MCH_2^+ (M = Cr, Mn, Co, Ni), showing a strong metal–methylene bond, 65–96 kcal mol^{-1}, are now available.[4] The $FeCH_2$ and $CuCH_2$ species have been isolated and characterized via FTIR matrix isolation spectroscopy.[5] The $(MCH_2)^+$ (M = Cr, Mn, Ru), and MCH_2 (M = Ni, Mn, Cu) complexes have been studied theoretically.[2c,d,h,6-13]

Taking into consideration the experience to date, the ground state of the $(MCH_2)^+$ complexes studied upto now, where the symbol M names a transition metal, can be described in terms of the interaction between the charged metal ground state, and the $^3B_1$ methylene ground state, leading to covalent M–C σ- and π-bonds (metal–alkylidene bonding). The interaction of a metal with the $^1A_1$ methylene low-lying excited state (metal–carbene bonding) has also been the subject of theoretical attention. In the case of $(RuCH_2)^+$,[12] several degenerate excited states showing

† Secció Departamental de Química-Física, Col. legi Universitari de Castelló de la Plana, Universitat de València, Apartat 224, Castelló de la Plana 12080, Spain.

(1) See, e.g.: Heck, R. F. *Organotransition Metal Chemistry*; Academic Press: New York, 1974.
(2) (a) Muetterties, E. L.; Stein, J. *Chem. Rev.* **1979**, *79*, 479. (b) Rofer-DePoorter, C. K. *Chem. Rev.* **1981**, *81*, 447. (c) Spangler, D.; Wendoloski, J. J.; Dupuis, M.; Chen, M. M. L.; Schaefer H. F., III. *J. Am. Chem. Soc.* **1981**, *103*, 3985. (d) Rappé, A. K.; Goddard, W. A., III. *J. Am. Chem. Soc.* **1982**, *104*, 448. (e) Henrici-Olivé, G.; Olivé, S. *J. Mol. Catal.* **1982**, *17*, 89. (f) Henrici-Olivé, G.; Olivé, S. *J. Phys. Chem.* **1984**, *88*, 2426. (g) Doyle, M. P. *Chem. Rev.* **1986**, *86*, 919. (h) Carter, E. A.; Goddard W. A., III. *J. Am. Chem. Soc.* **1987**, *109*, 579.
(3) See, e.g.: (a) Nitchké, F.; Ertl, G.; Küppers, J. *J. Chem. Phys.* **1981**, *74*, 5911. (b) Canning, N. D. S.; Madix, R. J. *J. Phys. Chem.* **1984**, *88*, 2437. (c) Schaefer, H. F., III. *Acc. Chem. Res.* **1977**, *10*, 287.
(4) (a) Armentrout, P. B.; Beauchamp, J. L. *J. Chem. Phys.* **1981**, *74*, 2819. (b) Armentrout, P. B.; Halle, L. F.; Beauchamp, J. L. *J. Am. Chem. Soc.* **1981**, *103*, 6501. (c) Halle, L. F.; Armentrout, P. B.; Beauchamp, J. L. *J. Am. Chem. Soc.* **1981**, *103*, 962.
(5) (a) Chang, S.-C.; Kafafi, Z. H.; Hauge, R. H.; Billups, W. E.; Margrave, J. L. *J. Am. Chem. Soc.* **1985**, *107*, 1447. (b) Chang, S.-C.; Kafafi, Z. H.; Hauge, R. H.; Billups, W. E.; Margrave, J. L. *J. Am. Chem. Soc.* **1987**, *109*, 4508.
(6) Rappé, A. K.; Goddard, W. A., III. *J. Am. Chem. Soc.* **1977**, *99*, 3966.
(7) (a) Brooks, B. R.; Schaefer, H. F., III. *Mol. Phys.* **1977**, *34*, 193. (b) Brooks, B. R.; Schaefer, H. F., III. *Int. J. Quantum Chem.* **1978**, *14*, 603.
(8) Vincent, M. A.; Yoshioka, Y.; Schaefer, H. F., III. *J. Phys. Chem.* **1982**, *86*, 3905.
(9) Carter, E. A.; Goddard, W. A., III. *J. Phys. Chem.* **1984**, *88*, 1485.
(10) Alvarado-Swaisgood, A. E.; Allison, J.; Harrison, J. F. *J. Phys. Chem.* **1985**, *89*, 2517.
(11) Carter, E. A.; Goddard, W. A., III. *J. Am. Chem. Soc.* **1986**, *108*, 4746.
(12) Carter, E. A.; Goddard, W. A., III. *J. Am. Chem. Soc.* **1986**, *108*, 2180.
(13) (a) Planelles, J.; Merchán, M.; Tomás, F. *Chem. Phys. Lett.* **1988**, *149*, 222. (b) Mochizuki, Y.; Tanaka, K.; Ohno, K.; Tatewaki, H.; Yamamoto, S. *Chem. Phys. Lett.* **1988**, *152*, 457.

0022-3654/89/2093-6596$01.50/0